Mn segregation dependence of damping capacity of as-cast M2052 alloy

Zhenyu Zhong,[1,a] Wenbo Liu,[1,a,b,*] Ning Li,[a,*] Jiazhen Yan,[a] jinwu Xie,[a] Dong Li,[a]

Ying Liu,[c] Xiuchen Zhao,[c] and Sanqiang Shi[b]

[a] School of Manufacturing Science and Engineering, Sichuan University,

Chengdu, 610065, P. R. China

[b] Department of Mechanical Engineering, The Hong Kong Polytechnic University,

Hung Hom, Kowloon, Hong Kong

[c] School of Materials Science and Engineering, Beijing Institute of Technology,

Beijing 100081, PR China

[1] These authors contributed equally.

Tel: +86-028-85405320; Fax: +86-028-85403408; E-mail: liuwenbo_8338@163.com.

Abstract

In this paper, three types of sand-casting M2052 alloys subjected to different heat treatments have been designed and prepared in order to investigate the relationship between Mn segregation and damping capacity using dynamic mechanical analysis, optical microscopy, X-ray diffraction, scanning electron microscopy, and energy dispersive spectroscopy. The results show that damping capacity has a crucial dependence on the Mn segregation in as-cast M2052 alloy. The original as-cast alloy without subsequent heat treatment shows its internal friction (Q^{-1}) is 1.52×10^{-2} at a strain amplitude of $\gamma=2\times10^{-4}$, while a remarkable enhancement (2.6×10^{-2}) of Q^{-1} can be obtained by ageing of the as-cast alloy at 435℃ for 4 hrs. This is mainly ascribed to the further formation of nanoscale Mn segregation in the Mn dendrites (so-called Mn macrosegregation) by spinodal decomposition during the ageing. On the contrary, performing the additional homogenization treatment at 850℃ for 24 hrs prior to the ageing at 435℃ for 4 hrs for the as-cast M2052 alloy can result in the obvious reduction of damping capacity (only 6.5×10^{-3} for Q^{-1}), which is closely associated with the distinct decrement of lattice distortion of γ'-Mn during f.c.c-f.c.t phase transformation caused by weakening of Mn segregation at the macro/nano-scale.

Keywords: Non-ferrous alloys; Casting; Internal friction; Ageing; Spinodal decomposition; Phase transformation

1. Introduction

Manganese-copper based alloys, well-known as the twinning interfaces type high damping materials, have been extensively studied for their antiferromagnetic transformation and phase transformation from face centered cubic to face centered tetragonal (f.c.c-f.c.t) [1-3]. The high damping capacity can be attributed to the mobility of internal boundaries, mainly including the {110} twin boundaries and phase boundaries [4,5]. Typically, the {110} twinning microstructure can readily be obtained in quenched Mn-Cu alloys with more than 82 at.% Mn by f.c.c-f.c.t phase transformation [6]. However, the high Mn content in the alloy matrix is fatally detrimental to the mechanical behaviors of Mn-Cu alloys, which will go against their practically industrial applications. It has been reported that for Mn-Cu alloys with relatively low Mn content, carrying out ageing treatment at a proper temperature range can form nanoscale Mn-enrichment through spinodal decomposition, which can markedly improve the damping capacity through the enhancement of f.c.c-f.c.t phase transition temperature (T_t) [7]. Obviously, this is an effective approach to achieve both high damping capacity and good mechanical property.

Among various of Mn-Cu damping alloys with low Mn contents, the M2052 alloy (Mn-20Cu-5Ni-2Fe, at.%) developed by Kawahara et al. shows a broad temperature stability for damping capacity and mechanical property [8]. Generally, the M2052 alloy ignots are forged or hot-rolled into bars and plates firstly and then carried out solution treatment to get γ-Mn phase, followed by ageing treatment. However, with the rapid development of industrialization, one-step molding casting has thus far

received considerable recognition for the distinct advantages of simple manufacturing process, low integrated cost and high production efficiency in comparison with forged alloys. Moreover, the solidification cooling rates varying in the range of 250~0.1 K/s have a significant influence on the damping capacity of as-cast M2052 alloy, and the T_t can be markedly improved in the slow cooled alloy owing to larger dendrite arm spacings [9]. Inspired by it, it can be easy to consider that although sand-casting is an ancient technology, it could act as a simple and effective approach to realize the excellent damping capacity for the as-cast M2052 alloy due to its very slow cooling rate during casting solidification compared to other casting methods. Also, to the best of our knowledge, little attention has so far been paid to the influence of ageing on the damping capacity of as-cast M2052 alloy, which is the Mn segregation dependence in essence.

In this report, three types of sand-casting M2052 alloys subjected to different heat-treatments have been well-designed and prepared to investigate the relationship between Mn segregation and damping capacity. The results show that damping capacity has a crucial dependence on the Mn segregation in as-cast M2052 alloy. Compared to the original as-cast alloy, a significant improvement of Q^{-1} can be obtained by ageing at 435℃ for 4 hrs due to the occurrence of higher Mn segregation at the nanoscale in the Mn dendrites, while weakening of Mn segregation through homogenization treatment prior to the ageing can result in the obvious reduction of damping capacity. Based on our understanding of damping machanism of as-cast Mn-Cu alloys, the probably reasons are discussed in detail accordingly.

2. Experimental procedure

Mn-20at.%Cu-5at.%Ni-2at.%Fe (M2052) alloy ingots were prepared by vacuum induction melting with pure metals in an inert argon atmosphere. The molten alloy was cast into the salica-sand mold through a sprue to get slow cooling rate, and then the sprue of ingots was cut out.

The specimens from the ingots were subjected to different heat treatments and then divided into three types assigned as 1#, 2# and 3#, respectively. Table 1 shows the detailed heat treatment conditions for each type of specimen, in which specimen 1# is the original as-cast M2052 alloy without subsequent heat treatment as the reference, as well as the specimens 2# and 3# were designed to achieve different Mn segregation under different heat treatment conditions.

For metallographic observation, all specimens were etched in a mixed solution of 10 g $FeCl_3.H_2O$, 30 ml HCl (37.5 wt.%) and 120 ml CH_3OH after mechanical polishing. Dendrite microstructure and composition distribution of specimens were characterized and analyzed using scanning electron microscopy (SEM, TESCAN VEGA II) equipped with energy dispersive spectroscopy (EDS). The phase structure and lattice parameters of specimens were identified by X-ray diffraction (XRD, Panalytical X'pert Pro X-Ray diffractometer, operated at 40 kV and 40 mA) with Cu Kα radiation, and all the diffraction profiles were obtained in continuous modes at a scan speed of 2 °/min. The specimens for XRD measurement, in sizes of 10×10×1 mm^3, were carefully prepared to remove surface strain.

Dynamic Mechanical Analysis (DMA, Q800 TA) was used for damping capacity

measurement of specimens. Each specimen under dual-cantilever mode possessed a dimension of 0.8×10×40 mm^3, and the resonant frequency and testing temperature were 1 Hz and 25 ℃, respectively. When the applied strain amplitude at the specimen surface varying from 0 to 2.5×10^{-4}, the damping capacity of the experimental alloy is characterized by internal friction Q^{-1} ($Q^{-1}=\tan\delta$, as described detailedly in the Ref. [10]).

3. Results and discussion

Fig.1 shows the strain-amplitude dependence of Q^{-1} of as-cast M2052 alloys subjected to different heat treatments at a test frequency of 1 Hz. It is clear that all the three specimens exhibit the strain-amplitude-dependent damping capacity with similar change tendency, among which the ageing specimen possesses the strongest strain-amplitude dependence of Q^{-1}. At the typical strain-amplitude of $\gamma=2\times10^{-4}$, the Q^{-1} is 1.52×10^{-2}, 6.5×10^{-3} and 2.6×10^{-2} for specimens 1#-3#, respectively. It indicates that the original as-cast M2052 alloy has certain damping capacity, which can be further improved by ageing at 435℃ for 4 hrs, while it decreases obviously as carrying out homogenization treatment at 850℃ for 24 hrs before the ageing. It is worthwhile noting that the present results are almost comparable with those obtained in the conventional as-forged M2052 alloys in our previous works [11-13], but in contrast the sand-casting technique used in this study has more evident advantages of simplicity, economy and efficiency.

Fig. 2 shows the metallographic micrographs of as-cast M2052 alloys subjected to different heat treatments. The obvious dendritical microstructures composed of dark

dendrites with lengths of about a few millimeters and widths of several micrometers as well as light interdendritic spacings can be observed in the specimen 1#, in which the dark regions are Mn-rich dendrites and the light areas are Cu-rich spacings. This is because the slow cooling rate of sand-casting induces the occurrence of casting segregation during the solidification of M2052 alloy and results in the formation of dendrite microstructures, in which dendrites can be precipitated primarily from liquid phase due to the higher melting point by Mn-enrichment and then Cu-rich spacings formed among them with the further decrease of temperature.

Compared to the specimen 1#, the casting segregation of specimen 2# is markedly weakened by homogenization-ageing treatment of as-cast M2052 alloy. Evidently, there is a large difference in the amounts and dimensions of Mn dendrites between specimens 1# and 2#. In contrast, the dendritical microstructure feature of as-cast M2052 alloy directly subjected to ageing treatment at 435℃ for 4 hrs (specimen 3#) has no evident difference in comparison with the original as-cast alloy. The present experimental results demonstrate that dendrite segregation can be essentially reduced by homogenization treatment of as-cast alloy for a relatively long time.

Fig. 3a shows the XRD patterns of as-cast M2052 alloys subjected to different heat treatments. It can be seen that f.c.c γ-Mn, f.c.t γ'-Mn and b.c.c α-Mn phases co-exist in the three types of specimens, correspondingly assigned to the diffraction peaks of (111), (200), (220) and (311) planes of γ-Mn, (202) and (220) planes of γ'-Mn, as well as (114) and (233) planes of α-Mn, respectively. Aside from the parent phase γ-Mn, the precipitated α-Mn phase in Mn dendrites is paramagnetic and cannot contribute to

the improvement of damping capacity, while the produced γ'-Mn by f.c.c-f.c.t phase transformation is antiferromagnetic and plays a key role to the damping capacity. It has been known that when the Mn-enrichment in the γ-Mn matrix is sufficient enough, the T_t can be raised to above room temperature and twinning plates of produced γ'-Mn tend to develop in a self-accommodation manner [6]. Typically, the c axis of γ'-Mn lattice is compressed and the a axis is elongated, resulting in the c/a ratio less than 1, which can be also confirmed by the obvious splits of {220} characteristic peak shown in Fig. 3b. Moreover, it is well-recognized that the dimensions change of c and a axes of γ'-Mn lattice can be featured as lattice distortion (*a*/*c*-1), which can be calculated quantitatively by the Equation (1) below:

$$\frac{1}{d^2} = \frac{H^2+K^2}{a^2} + \frac{L^2}{c^2} \quad (1)$$

where d refers to the interplanar spacing of (H K L) plane of γ'-Mn, a and c to the lattice parameters of γ'-Mn. According to the Equation (1), the a and c values for three specimens can be estimated by the split peak positions of {220} peak in the XRD patterns, as listed detailedly in Table 2. Obviously, the largest lattice distortion of γ'-Mn during the f.c.c-f.c.t phase transformation can be obtained in the specimen 3#, which would be accountable for the optimal damping capacity, as discussed in detail in the following section.

Fig. 4 further presents the relationship between lattice distortion (*a*/*c*-1) and damping capacity (Q^{-1}, at a strain amplitude of $\gamma=2\times10^{-4}$) of as-cast M2052 alloys subjected to different heat treatments. As can be seen clearly, the lattice distortion has a positive correlation to damping capacity, namely the larger the lattice distorition is,

the better the damping capacity is. According to the Cochardt's magnetomechanical damping model [14], the damping capacity has a positive association with saturation magnetostriction constant (λ) under the same strain amplitude. The value of λ can be estimated well by mean of the lattice parameters (a and c) of γ'-Mn through Equation (2) as follows [15]:

$$\lambda = \frac{1}{4} V_f \left(\frac{a-c}{c}\right) \quad (2)$$

where V_f denotes the total volume fraction of antiferromagnetic Mn-rich regions. Obviously, in this case, the λ is proportional to *a/c*-1 due to the negligible difference in V_f based on the XRD results in Fig. 4. Thus, the larger the lattice distorition is, the greater the λ is, and the better the damping capacity is.

Fig. 5 shows the SEM micrographs of as-cast M2052 alloys without subsequent heat treatment and with homogenization at 850℃ for 24 hrs followed by quenching into cool water, respectively. The micron-sized Mn-rich dendrites and Cu-rich interdendritic spacings can be observed clearly in the original as-cast M2052 alloy, while no distinct dendrite microstructure can be found in the homogenized as-cast M2052 alloy. Table 3 further shows the compositional EDS analysis corresponding to typical Mn-rich and Cu-rich regions marked in Fig. 5. It can be easy to find that the average Mn content in Mn-rich regions of as-cast M2052 alloy is 82.52 at.%, while it markedly decreases to 74.30 at.% after homogenization, just slightly higher than designed Mn content of M2052 alloy, indicating that homogenization treatment can give rise to the obvious reduction of Mn segregation in the dendrites of as-cast M2052 alloy.

It has been known that the lattice distortion of γ'-Mn during f.c.c-f.c.t phase transformation in Mn-Cu alloys takes place below T_t, and T_t is crucially dependent on the Mn content in Mn-Cu alloys [16]. The higher the Mn content is, the higher the T_t is, the larger the lattice distortion is, and thus the better the damping capacity would be. Moreover, when Mn-Cu alloys are subjected to ageing at the temperature range of miscibility gap (400℃~600℃), the γ-Mn parent phase can be broken up into Mn-enrichment and Cu-enrichment at the nanoscale through spinodal decomposition due to the decrease of strain energy, typical of 'tweed' microstructure [17-19]. In this case, nanoscale Mn segregation can be further achieved in the Mn dendrites of as-cast M2052 alloy by spinodal decomposition upon ageing at 435℃ for 4hrs. Thus, the content of Mn in Mn-rich regions of specimen 3# is extremely high, which is responsible for the larger lattice distortion and the better damping capacity.

On the other hand, it has been reported that if f.c.t γ'-Mn phase can be formed at room temperature, the Mn concentration (C_{Mn}) in nanoscale Mn-rich regions after spinodal decomposition must be beyond 83.4 %, and the quantitative relationship between C_{Mn} and tetragonality c/a can be expressed as [20]:

$$c/a = 2.638 - 3.317c_{Mn} + 1.618c_{Mn}^2 \qquad (3)$$

According to the calculated a and c values of γ'-Mn for three specimens in Table 2, C_{Mn} in nanoscale Mn-rich regions upon spinodal decomposition can be further estimated for each specimen, as listed in Table 4. For further comparison, the average Mn content in Mn dendrites before spinodal decomposition for each specimen can be obtained from the EDS results in Table 3 and simultaneously presented in Table 4.

Evidently, the highest Mn content in nanoscale Mn-rich regions after spinodal decomposition can be acquired in the specimen 3#, while homogenization-ageing treatment results in both the lowest average Mn content in Mn dendrites before spinodal decomposition and the lowest C_{Mn} in nanoscale Mn-rich regions after spinodal decomposition among these three specimens, implying the smallest lattice distortion of γ'-Mn and the worst damping capacity for the specimen 2#. Furthermore, it is worthwhile noting that the spontaneous spinodal decomposition process for a relatively short period still can occurred in the original as-cast M2052 alloy during casting solidification due to the very slow cooling rate of sand-casting, which is the reason that there is a little difference between the average Mn content in Mn dendrites and the C_{Mn} in nanoscale Mn-rich regions for the specimen 1#.

Based on our current experimental results, it can be proposed that the damping capacity has a crucial dependence on the Mn segregation in as-cast M2052 alloy, and thus adjusting and controlling of Mn segregation can effectively improve the damping capacity. Ageing is beneficial for the formation of nanoscale Mn-rich regions by spinodal decomposition and further enhances the Mn segregation degree in as-cast M2052 alloy, resulting in the raise of f.c.c-f.c.t phase transition temperature and the increase of lattice distortion, eventually improving the damping capacity markedly. On the contrary, homogenization treatment can weaken the Mn segregation in as-cast M2052 alloy, including in the Mn dendrites and nanoscale Mn-rich regions, hence essentially lowering the damping capacity. This work has an important implication for design and preparation of high-performance Mn-Cu damping alloys for practical

industrial applications.

4. Conclusion

In Summary, the relationship between Mn segregation in as-cast M2052 alloy and its damping capacity has been investigated systematically through designing and carrying out different heat treatment processes. The damping capacity has a crucial dependence on the Mn segregation in as-cast M2052 alloy. Compared to the original as-cast alloy with Q^{-1} of 1.52×10^{-2} at $\gamma=2\times10^{-4}$, a remarkable improvement of damping capacity ($Q^{-1}=2.6\times10^{-2}$) can be obtained by ageing at 435℃ for 4 hrs. This can be attributed to the further formation of nanoscale Mn segregation in the Mn dendrites through spinodal decomposition during the ageing. On the contrary, carrying out the additional homogenization treatment at 850℃ for 24 hrs prior to the ageing can result in the obvious reduction of damping capacity of as-cast M2052 alloy (only 6.5×10^{-3} for Q^{-1}), which is closely related to the distinct decrement of lattice distortion of γ'-Mn during f.c.c-f.c.t phase transformation by weakening of Mn segregation at both the macro- and nano-scale.

Acknowledgements

We give thanks to financial support by the National Natural Science Foundation of China (11076109), the "HongKong Scholars Programme" Funded Project (XJ2014045, G-YZ67), the China Postdoctoral Science Foundation Funded Project (2015M570784), the Scientific Research Fund of Sichuan Provincial Department of Education (16ZB0002), and the Talent Introduction Program of Sichuan University (YJ201410).

References

[1] F.T. Worrell, J. Appl. Phys. 19 (1948) 929-933.

[2] G.E. Bacon, I.W. Dunmur, J.H. Smith, R. Street, Proc. R. Soc. London, Ser. A 241 (1957) 223-238.

[3] F.X. Yin, Y. Ohsawa, A. Sato, K. Kawahara, Acta Mater. 48 (2000) 1273-1282.

[4] J.M. Vitek, H. Warlimont, Met. Sci. 10 (1976) 7-13.

[5] C.P. Wang, X.J. Liu, I. Ohnuma, R. Kainuma, K. Ishida, J. Alloys Compd. 438 (2007) 129-141.

[6] A.V. Siefert, F.T. Worrell, J Appl. Phys. 22 (1951) 1257-1259.

[7] K. Tsuchiya, H. Sato, S. Edo, K. Marukawa, M. Umemoto, Mater. Sci. Eng. A 285 (2000) 353-356.

[8] F.X. Yin, Acta Metall. Sin. 39 (2003) 1139-1144.

[9] F.X. Yin, I.S. Shi, S Akuya, S. Takuya, N. Kotobu, Prog. Phys. 9 (2006) 323-331.

[10] G. Haneczok, M. Weller, Mater. Sci. Eng. A 370 (2004) 209-212.

[11] J.Z. Yan, N. Li, X. Fu, W.B. Liu, Y. Liu, X.C. Zhao, Adv. Eng. Mater. 17 (2015) 1332-1337.

[12] J.Z. Yan, N. Li, X. Fu, Y. Zhang, Mater. Sci. Eng. A 618 (2014) 205-209.

[13] Y. Zhang, N. Li, J.Z. Yan, J.W. Xie, Adv. Mater. Res. 873 (2014) 36-41.

[14] G.W. Smith, J.R. Birchak, J. Appl. Phys. 39 (1968) 2311-2316.

[15] S. Laddha, D.C. Van-Aken, Metall. Mater. Trans. A 26 (1995) 957-964.

[16] F.X. Yin, Y. Ohsawa, A. Sato, K. Kawahara, Mater. Trans., JIM 40 (1999) 451-454.

[17] F. Findik, Mater. Design 42 (2012) 131-146.

[18] O. Soriano-Vargas, E.O. Avila-Davila, V.M. Lopez-Hirata, N. Cayetano-Castro, J.L. Gonzalez-Velazquez, Mater. Sci. Eng. A 527 (2010) 2910-2914.

[19] G.V. Markova, D.M. Levin, S.E. Kazharskaya, E.S. Klyueva, G.M. Tateladze, E.A. Bannikova, I.K. Popovichenko, Mater. Today Proceedings 2 (2015) S841-S844.

[20] N. Cowlam, G.E. Bacon, L. Gillott, J. Phys. F: Met. Phys. 7 (1977) L315-L319.

Figure Captions:

Fig. 1. Strain-amplitude dependence of Q^{-1} of as-cast M2052 alloys subjected to different heat treatments at a test frequency of 1 Hz.

Fig. 2. Metallographic micrographs of as-cast M2052 alloys subjected to different heat treatments.

Fig. 3. (a) XRD patterns of as-cast Mn2052 alloys subjected to different heat treatments; (b) Clear splits of {220} characteristic peaks at a high-magnification.

Fig. 4. The relationship between lattice distortion (*a/c*-1) and damping capacity (Q^{-1}, at a strain of $\gamma=2\times10^{-4}$) of as-cast M2052 alloys subjected to different heat treatments.

Fig. 5. SEM micrographs of as-cast M2052 alloys (a) without subsequent treatment and (b) with homogenization at 850℃ for 24 hrs followed by quenching into cool water. The broken lines in part b indicate the indistinct dendrites.

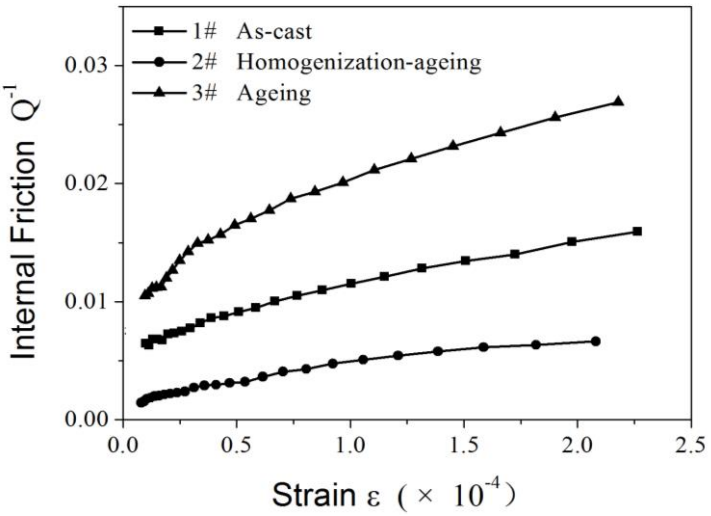

Fig. 1. Strain-amplitude dependence of Q^{-1} of as-cast M2052 alloys subjected to different heat treatments at a test frequency of 1 Hz.

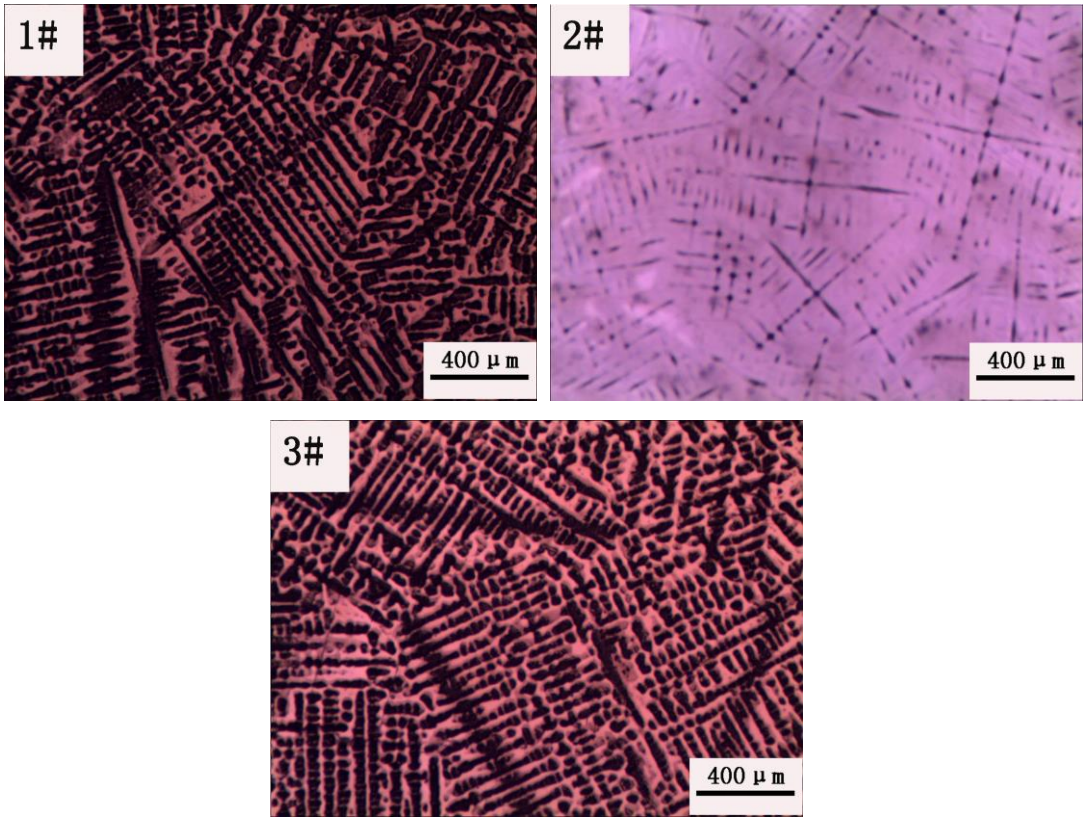

Fig. 2. Metallographic micrographs of as-cast M2052 alloys subjected to different heat treatments.

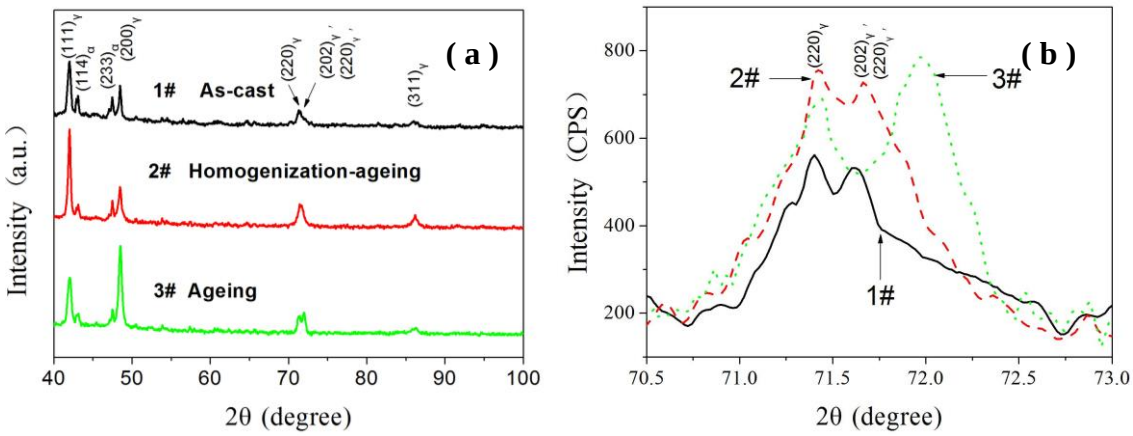

Fig. 3. (a) XRD patterns of as-cast Mn2052 alloys subjected to different heat treatments; (b) Clear splits of {220} characteristic peaks at a high-magnification.

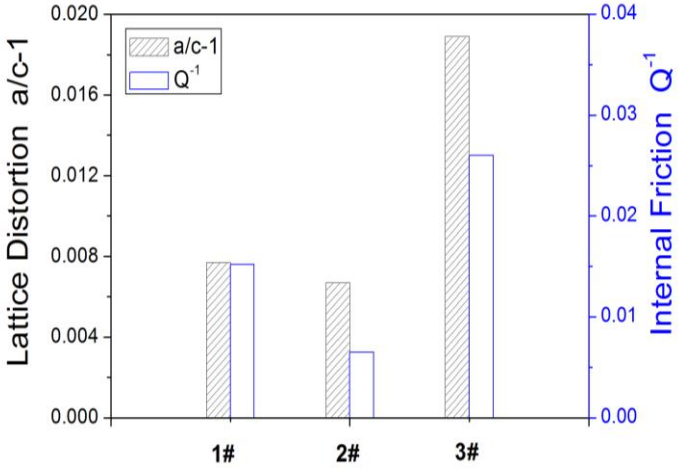

Fig. 4. The relationship between lattice distortion (*a*/*c*-1) and damping capacity (Q^{-1}, at a strain of $\gamma=2\times10^{-4}$) of as-cast M2052 alloys subjected to different heat treatments.

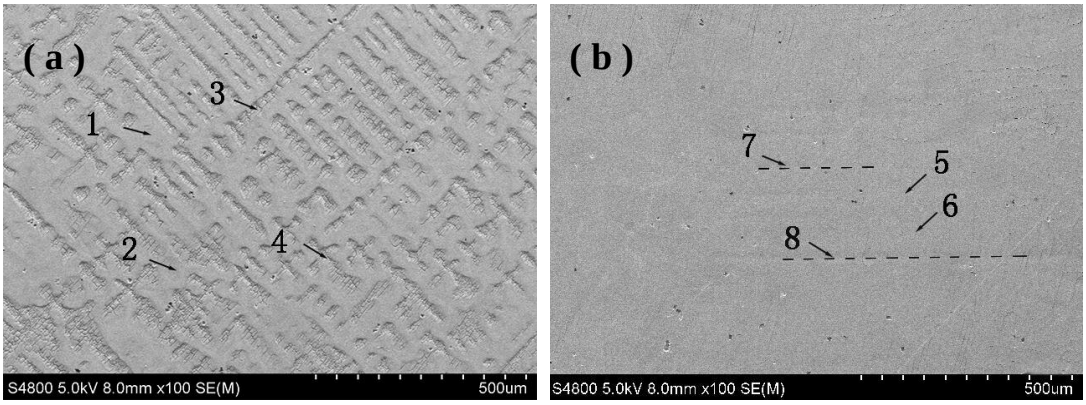

Fig. 5. SEM micrographs of as-cast M2052 alloys (a) without subsequent treatment and (b) with homogenization at 850℃ for 24 hrs followed by quenching into cool water. The broken lines in part b indicate the indistinct dendrites.

Table 1. Detailed heat treatment conditions of three types of specimens.

Specimens	Heat treatment conditions
1#	Original as-cast alloy without subsequent heat treatment
2#	Homogenizing at 850℃ for 24 hrs, and then quenching into cool water before ageing at 435℃ for 4 hrs (homogenization-ageing treatment)
3#	Ageing at 435℃ for 4 hrs

Table 2. Calculated lattice parameters and lattice distortion of as-cast M2052 alloys subjected to different heat-treatments by Equation (1).

Specimens	Lattice parameters [Å]				Lattice Distortion
	Indexed Interplanar spacing		Calculated lattice parameter		
	d_{220}	$d_{022\&202}$	a	c	a/c-1
1#	1.3214	1.3163	3.7375	3.7088	0.0077
2#	1.3191	1.3147	3.7310	3.7062	0.0067
3#	1.3192	1.3068	3.7313	3.6621	0.0189

Table 3. Compositional EDS analysis corresponding to typical Mn-rich and Cu-rich regions in Fig. 5.

	Region	Site	Mn (at.%)	Cu (at.%)	Ni (at.%)	Fe (at.%)
Fig. 5a	Cu-enrichment	1	64.12	30.27	3.97	1.64
		2	63.66	29.45	4.88	2.01
	Mn-enrichment	3	82.72	12.07	4.07	1.14
		4	82.32	12.46	4.12	1.10
Fig. 5b	Cu-enrichment	5	69.41	24.58	4.01	2.00
		6	70.10	22.92	5.01	1.97
	Mn-enrichment	7	74.50	19.91	4.44	1.15
		8	74.09	19.68	4.51	1.71

Table 4. Comparison between average Mn content in Mn dendrites before spinodal decomposition and C_{Mn} in nanoscale Mn-rich regions after spinodal decomposition (at.%).

Specimens	1#	2#	3#
Average Mn content in Mn dendrites before spinodal decomposition	82.52	74.30	82.52
C_{Mn} in nanoscale Mn-rich regions after spinodal decomposition	84.23	83.99	86.12